Investigation on the reflection at the boundaries for reconstruction laser-based imaging

Boulanger, Joan; Liu, Fengshan; Charette, André

Publisher's version / Version de l'éditeur:
http://dx.doi.org/10.1016/j.jqsrt.2006.07.014
Journal of Quantitative Spectroscopy and Radiative Transfer, 104, 2, pp. 238-247

ELSEVIER

Journal of Quantitative Spectroscopy & Radiative Transfer 104 (2007) 238–247

Journal of Quantitative Spectroscopy & Radiative Transfer

www.elsevier.com/locate/jqsrt

Investigation on the reflection at the boundaries for reconstruction laser-based imaging

Joan Boulanger[a,*], Fengshan Liu[a], André Charette[b]

[a]*National Research Council Canada, Institute for Chemical Process and Environmental Technology, Montréal Road, Building M9, Ottawa, Ont, Canada K1A 0R6*

[b]*Groupe de Recherche en Ingénierie des Procédès et Systèmes, Département des Sciences Appliquées, Université du Québec à Chicoutimi, Boulevard de l'Université, Chicoutimi, Québec, Canada G7H 2B1*

Received 10 July 2006; accepted 28 July 2006

Abstract

Optical tomography is acknowledged as an economic and harmless probing technique for medical applications. Recent research tends to show that the use of long term photons, which have travelled a long time in the whole sample to be probed, carry more information in the image reconstruction process. Numerical simulations based on short-pulsed laser beam interaction with non-homogeneous matter are presented. The aim is to emphasize the effect of reflective boundary conditions since reflection enforces photons to stay for a longer period of time in the phantom. It is found that the quality of reconstruction is better when the boundaries are reflecting.

Keywords: Optical tomography; Inverse problem; Imaging; Boundary conditions

1. Introduction

Among the new imaging modalities expected to be available in the future, optical tomography is one of the most promising although numerous difficulties still exist. The interest in optical tomography lies in the nature of the radiation. As the name indicates, visible or infrared radiation (non-ionizing) is used. Hence, equipment based on such technology is expected to be easy to handle, thus cheaper, while being harmless for the object to be probed. Low spatial resolution of this imaging method appears for media with high scattering properties, as in biological tissues, which make light propagation a diffuse process. The medium is said to be a *low-pass filter*.

In direct tomography, measured transmitted or/and reflected signals are processed in order to extract some information about the inside of a semi-transparent medium to which a laser beam has been applied. This may be the case when back-projection of the transmitted light is used along the collimated beam direction or when the apparent time-of-flight of photons is employed. In that sense, optical tomography may be compared to X-ray computer tomography [1]. In a material with a high level of scattering, direct tomography is of limited use

*Corresponding author. National Research Council Canada, Institute for Aerospace Research, Building M-10, 1200 Montréal Road, Canada.

E-mail address: Joan.Boulanger@nrc-cnrc.gc.ca (J. Boulanger).

0022-4073/$ - see front matter
doi:10.1016/j.jqsrt.2006.07.014

Nomenclature

Only symbols that are either not available or different from those in the international nomenclature of thermal sciences are listed.

D	Domain
∂D	Geometrical boundary
F	Analytic filter
S	Energy source term
T	Time interval
d	Detector reading
$\vec{d}$	Search direction
$\mathrm{d}\vec{r}_{\mathrm{b}}$	Outgoing elementary surface
$\mathrm{d}\vec{r}$	Elementary volume
$\vec{n}$	Outgoing normal to surface
$\vec{r}$	Position vector
$t_{\max}$	End time
t_{travel}	Time to cross the medium

Greek Letters

Δ	Variation
α	Descent step
φ	Objective function
λ	Lagrangian multiplier

Superscripts

M	Measurement
P	Prediction
c	Collimated variable
k	Reconstruction step
0	Reference value
*	Non-dimensional variable
$'$	Incident direction

Subscripts

b	Boundary
i	Node

because photons do not travel along a straight line and the reconstruction is made non-linear, which prohibits the use of direct reconstruction methods such as the Radon transform. Devices such as time-gating techniques [2] and spatial filtering [3] have been developed to track the less scattered photons (the ones following as close as possible the collimated direction) but the high extinction precludes the probing of thick media. Other authors have made use of the apparent path of the photons due to the numerous scattering events through the time-of-flight of the transmitted maximum of a laser impulsion [4]. The knowledge of this path is expected to provide empirical correlations for quantification of the data but no imaging has been developed based on this method. Hence, it is unlikely that remote probing methods utilizing the collimated beam may be useful for imaging in highly scattering semi-transparent media, like in biomedical tissues. This is the reason why researchers have explored means of using the diffuse part of the signal, since, in a highly scattering (but low

absorbing) medium, diffuse light carries not only the most energetic part of the signal but also the most informative part as well. This is due to the long travel these photons accomplish within the medium. A mean of making use of all the information embedded in the diffuse signal is the inverse problem applied to reconstruction tomography. Reconstruction tomography aims at deriving quantitative images of the optical properties distribution (σ_s and κ, respectively, the scattering and absorption coefficients, both in m^{-1}) of an irradiated medium given some measurements acquired at the boundary [5]. Other properties may also be obtained [6,7]. They make use of a transport model [8–10]. The experimental set-up consists of light guided by optical fibres to the surface of the sample and detecting fibres to collect the emerging light from the boundaries. When applied in the time domain, several studies, e.g. [11,12], have shown that filtering the data in favour of the long-term diffuse photons helps improve the quality of the reconstruction, for the same reason mentioned above.

For authors' best knowledge, effects of boundary conditions on the quality of imaging have not been investigated. Some studies have been done by considering boundaries, [7,8,10], while others not, [13,14], in the case of inverse problem analysis and numerous studies have investigated boundary conditions for the diffusion approximation, see a comprehensive development in [15], but the effect on imaging has not been elucidated. For inverse reconstruction problems, it is worth noting that reflective boundary conditions are a way to enforce photons to stay longer within the sample and should have the same effects as long-term filtering while being applicable to steady-state [16] or frequency-domain techniques [17], where time filtering is not available. It is also likely to improve or speed-up the reconstruction process.

The aim of this study is thus to numerically investigate the effect of the reflection at boundaries on the quality of reconstruction imaging. The task is purely numerical and the algorithm is detailed in [18]. The development recalled here concerns the introduction of boundary conditions. The next section is dedicated to the presentation of the algorithm. The last section presents reconstructions as in [19] and the accuracy of the reconstruction is studied with respect to the new boundary conditions.

2. Model problem

2.1. Forward algorithm

To treat the full hyperbolic nature of light pulse propagation in a semi-transparent medium, the time-dependent Boltzmann-type tRTE given below, [12,20], is retained with usual notations:

$$\frac{n}{c}\frac{\partial I}{\partial t}+\nabla\cdot\left(\vec{\Omega}\cdot I\right)+(\kappa+\sigma_s)I=\frac{\sigma_s}{4\pi}\int_{4\pi}\mathrm{d}\Omega'\Phi\left(\vec{\Omega}',\vec{\Omega}\right)I+\frac{\sigma_s}{4\pi}\,\Phi(\vec{\Omega}^c,\vec{\Omega})I^c. \tag{1}$$

The medium is non-emitting. I^c and $\vec{\Omega}^c$ are described in the next section.

2.1.1. Collimated irradiation

Energy enters the system through incident pulse irradiation, which is semi-analytically integrated on its straight characteristic path $\vec{\Omega}^c$. Energy lost by the beam is gained by the medium through absorption and injected in the field of induced radiation intensity through scattering. This is the role of the last term in Eq. (1). Bouguer–Beer–Lambert extinction law governs the collimated irradiation:

$$\frac{n}{c}\frac{\partial I^c}{\partial t}+\nabla\cdot\left(\vec{\Omega}^c\cdot I^c\right)+(\kappa+\sigma_s)I^c=0. \tag{2}$$

Similar treatments of boundary emanating radiation have already been introduced for the homogeneous case, [21–23], to counter the ray effect.

2.1.2. Initial and boundary conditions

Initially, there is no light (or photons) in the medium before irradiation impingement. The reflectivity (ρ) and transmitivity (τ) are obtained at the boundary according to the Fresnel-derived law presented below and

proposed in [9]:

$$\rho = \frac{\sin^2(\theta_1 - \theta_2) + \sin^2(\theta_1 + \theta_2)}{2\cos(\theta_1)}, \quad \tau = 1 - \rho\,\cos(\theta_1). \tag{3}$$

θ_1 is the angle with respect to the outgoing normal $\vec{n}$ of the impinging intensity from inside the sample. θ_2 is the corresponding refracted angle, following Descartes' law (incident, refracted and reflected beams are all included in a plane containing the local normal $\vec{n}$):

$$n\sin(\theta_1) = \sin(\theta_2). \tag{4}$$

The refractive index of the sample is n while the one of air is considered as unity.

Detectors are considered to have a full hemispherical aperture, nevertheless only the angles of emergence ($\tau > 0$) contribute to the signal. The boundary quantity that is measurable (the exitance) is defined as

$$\mathrm{d}(I) = \int_{\cos\left(\vec{\Omega}_1,\vec{n}\right)>0} \mathrm{d}\Omega_1 \tau\left(\vec{\Omega}_1\right) I\left(\vec{\Omega}_1\right) \cos\left(\vec{\Omega}_1,\vec{n}\right) + \tau\left(\vec{\Omega}_1^{\mathrm{c}}\right) I^{\mathrm{c}}\,\cos\left(\vec{\Omega}_1^{\mathrm{c}},\vec{n}\right)\Big|_{\cos\left(\vec{\Omega}_1^{\mathrm{c}},\vec{n}\right)>0}. \tag{5}$$

2.2. Inversion methods

Reconstruction optical spectroscopy is currently known as a process which allows the recovery of the optical properties σ_s and κ inside the irradiated medium, given some measurements acquired at the boundary. A forward model simulating light propagation in the medium for an initial guess of the optical properties is first used. The model employed here is the tRTE presented above with reflective boundary conditions. The predicted measurements at boundary surface are compared to the measured ones through an objective function (non-linear optimization). An inverse problem is then defined in order to line-minimize the objective function by finding its gradient in view of the numerous optical parameters distributed in the whole domain, leading to the reconstruction of the unknown optical properties distribution. The imaging contrast is directly given by one or several optical properties maps, helping find the information inside the object to be probed.

Hemispherical detector measurements predicted by the forward code presented above, Eq. (5), are compared to the actual ones collected at the medium surface through the objective square error function ϕ:

$$\phi = \frac{1}{2}\int_T \mathrm{d}t \int_{\partial D} \mathrm{d}\vec{r}_{\mathrm{b}} \left(F(d^{\mathrm{P}}) - F(d^{\mathrm{M}})\right)^2, \tag{6}$$

where $\vec{r}_{\mathrm{b}}$ identifies the position on the boundary elementary surface $\mathrm{d}\vec{r}_{\mathrm{b}}$, F is a function to filter the data, superscript P refers to the readings predicted by the forward model while M represents the measured ones. Symbol ∂D designates the integration over the whole boundary (of domain D) positions where detectors are located. Summation over the time period T is for the detector time dependent sampling of the temporal signature. The reconstruction process aims at minimizing the objective function ϕ (Eq. (6)) using the line minimization technique (Polak–Ribière non-linear conjugate gradient for this study). The required quantity is thus the gradient of the objective function in the optical parameters space (κ, σ_s). The determination of this quantity is the key of the inversion algorithm and may be obtained through an adjoint model [8].

Adjoint models are derived by considering that the objective function (Eq. (6)) must be minimized under some constraints given by the radiative transfer equations for both the collimated and induced radiation. Those derivations are detailed in [19] and are not repeated here. After some algebra, gradients are explicitly given by

$$\frac{\mathrm{d}\phi}{\mathrm{d}\kappa} = \int_T \mathrm{d}t \int_{4\pi} \mathrm{d}\Omega\,\lambda I + \int_T \mathrm{d}t\,\lambda^{\mathrm{c}} I^{\mathrm{c}}, \tag{7}$$

$$\frac{\mathrm{d}\phi}{\mathrm{d}\sigma_s} = \int_T \mathrm{d}t \int_{4\pi} \mathrm{d}\Omega \left\{ \lambda I - \frac{\lambda}{4\pi}\int_{4\pi} \mathrm{d}\Omega'\,\Phi\left(\vec{\Omega}',\vec{\Omega}\right) I - \frac{\lambda}{4\pi}\,\Phi\left(\vec{\Omega}^{\mathrm{c}},\vec{\Omega}\right) I^{\mathrm{c}} \right\} + \int_T \mathrm{d}t\,\lambda^{\mathrm{c}} I^{\mathrm{c}} \tag{8}$$

and the following relation must be satisfied by the adjoint operator λ and λ^{c} to I and I^{c}, respectively:

$$
\begin{aligned}
0 = & \int_T \mathrm{d}t \int_{\partial D} \mathrm{d}\vec{r}_{\mathrm{b}} \left(F(d^{\mathrm{P}}) - F(d^{\mathrm{M}})\right) F' \left(\frac{\partial d^{\mathrm{P}}}{\partial I}\,\Delta I + \frac{\partial d^{\mathrm{P}}}{\partial I^{c}}\,\Delta I^{c}\right) \\
& + \int_T \mathrm{d}t \int_D \mathrm{d}\vec{r} \int_{4\pi} \mathrm{d}\Omega\, \lambda \left\{ \frac{n}{c}\frac{\partial \Delta I}{\partial t} + \overbrace{\nabla \cdot \left(\vec{\Omega}\cdot \Delta I\right)}^{\mathrm{I}} + (\kappa+\sigma_{\mathrm{s}})\Delta I \right. \\
& \left. - \frac{\sigma_{\mathrm{s}}}{4\pi}\int_{4\pi} \mathrm{d}\Omega'\, \Phi\left(\vec{\Omega}', \vec{\Omega}\right)\Delta I - \frac{\sigma_{\mathrm{s}}}{4\pi}\,\Phi\left(\vec{\Omega}^{c}, \vec{\Omega}\right)\Delta I^{c} \right\} \\
& + \int_T \mathrm{d}t \int_{D^{c}} \mathrm{d}\vec{r}^{c}\, \lambda^{c} \left\{ \frac{n}{c}\frac{\partial \Delta I^{c}}{\partial t} + \nabla \cdot \left(\vec{\Omega}\cdot \Delta I^{c}\right) + (\kappa+\sigma_{\mathrm{s}})\Delta I^{c} \right\}
\end{aligned}
\tag{9}
$$

Each term of Eq. (9) is transformed in order to derive the adjoint equation relative to the radiative transfer one, accounting to the boundary conditions:

$$
I_{\cos\left(\vec{\Omega},\vec{n}\right)<0} = \int_{\cos\left(\vec{\Omega}',\vec{n}\right)>0} \mathrm{d}\Omega' \rho\left(\vec{\Omega}', \vec{\Omega}\right) I\, \cos\left(\vec{\Omega}', \vec{n}\right). \tag{10}
$$

The adjoint derivation from Eq. (9) may be found in [19]. The particular interest here is the new reflective boundary conditions. Term (I) in Eq. (9) is thus recast into

$$
\int_T \mathrm{d}t \int_D \mathrm{d}\vec{r} \int_{4\pi} \mathrm{d}\Omega\, \lambda \nabla \cdot \left(\vec{\Omega}\cdot \Delta I\right) = \overbrace{\int_T \mathrm{d}t \int_{\partial D} \mathrm{d}\vec{r}_{\mathrm{b}} \int_{4\pi} \mathrm{d}\Omega\, \lambda \Delta I\, \cos\left(\vec{\Omega}\cdot\vec{n}\right)}^{\mathrm{II}} - \int_T \mathrm{d}t \int_D \mathrm{d}\vec{r} \int_{4\pi} \mathrm{d}\Omega\, \Delta I \nabla \cdot \left(\vec{\Omega}\cdot\lambda\right). \tag{11}
$$

Term (II) in Eq. (11) defines time-dependent boundary conditions for λ when balancing the first term on the right hand side of Eq. (9), which gives the residuals of the objective function. By identification, boundary conditions for λ are defined as follows:

$$
\begin{aligned}
& \int_T \mathrm{d}t \int_{\partial D} \mathrm{d}\vec{r}_{\mathrm{b}} \left(F(d^{\mathrm{P}}) - F(d^{\mathrm{M}})\right) F' \int_{\cos\left(\vec{\Omega},\vec{n}\right)>0} \mathrm{d}\Omega\, \tau\, \cos\left(\vec{\Omega}, \vec{n}\right)\Delta I \\
& \quad = -\int_T \mathrm{d}t \int_{\partial D} \mathrm{d}\vec{r}_{\mathrm{b}} \int_{\cos\left(\vec{\Omega},\vec{n}\right)>0} \mathrm{d}\Omega\, \lambda\, \cos\left(\vec{\Omega}, \vec{n}\right)\Delta I - \int_T \mathrm{d}t \int_{\partial D} \mathrm{d}\vec{r}_{\mathrm{b}} \int_{\cos\left(\vec{\Omega},\vec{n}\right)<0} \mathrm{d}\Omega\, \lambda\, \cos\left(\vec{\Omega}, \vec{n}\right)\Delta I.
\end{aligned}
\tag{12}
$$

The last term in Eq. (12) must be expressed using the boundary conditions expression Eq. (10):

$$
\begin{aligned}
& \int_T \mathrm{d}t \int_{\partial D} \mathrm{d}\vec{r}_{\mathrm{b}} \int_{\cos\left(\vec{\Omega},\vec{n}\right)<0} \mathrm{d}\Omega\, \lambda\, \cos\left(\vec{\Omega}, \vec{n}\right) \Delta I \\
& \quad = \int_T \mathrm{d}t \int_{\partial D} \mathrm{d}\vec{r}_{\mathrm{b}} \int_{\cos\left(\vec{\Omega},\vec{n}\right)<0} \mathrm{d}\Omega\, \lambda\, \cos\left(\vec{\Omega}, \vec{n}\right) \int_{\cos\left(\vec{\Omega}',\vec{n}\right)>0} \mathrm{d}\Omega'\, \rho\left(\vec{\Omega}', \vec{\Omega}\right) \cos\left(\vec{\Omega}', \vec{n}\right)\Delta I
\end{aligned}
\tag{13}
$$

which can be re-written as

$$
\int_T \mathrm{d}t \int_{\partial D} \mathrm{d}\vec{r}_{\mathrm{b}} \int_{\cos\left(\vec{\Omega}',\vec{n}\right)>0} \mathrm{d}\Omega'\, \Delta I\, \cos\left(\vec{\Omega}', \vec{n}\right) \int_{\cos\left(\vec{\Omega},\vec{n}\right)<0} \mathrm{d}\Omega\, \rho\left(\vec{\Omega}', \vec{\Omega}\right) \cos\left(\vec{\Omega}, \vec{n}\right). \tag{14}
$$

Eq. (12) combined with Eq. (14) readily gives the boundary closure for term (II) in Eq. (11). Boundary conditions for λ are in fact driven by the residuals of the transmitted readings obtained at the surface of the material and subject to the same laws of reflection as the intensity field.

The corresponding development for the collimated beam is straightforward. Adjoint equations to the radiative transfer ones for the collimated and in-scattered variables I^{c} and I are finally defined as

$$\frac{n}{c}\frac{\partial\lambda}{\partial t}-\nabla\cdot\left(\vec{\Omega}\cdot\lambda\right)+(\kappa+\sigma_{\mathrm{s}})\lambda-\frac{\sigma_{\mathrm{s}}}{4\pi}\int_{4\pi}\mathrm{d}\Omega'\,\Phi\left(\vec{\Omega},\vec{\Omega}'\right)\lambda=0\quad\text{on } D \tag{15a}$$

$$\frac{n}{c}\frac{\partial\lambda^{\mathrm{c}}}{\partial t}-\nabla\cdot\left(\vec{\Omega}^{\mathrm{c}}\cdot\lambda^{\mathrm{c}}\right)+(\kappa+\sigma_{\mathrm{s}})\lambda^{\mathrm{c}}-\frac{\sigma_{\mathrm{s}}}{4\pi}\int_{4\pi}\mathrm{d}\Omega\,\Phi\left(\vec{\Omega}^{\mathrm{c}},\vec{\Omega}\right)\lambda=0\quad\text{on } D^{\mathrm{c}} \tag{15b}$$

if reverse time from $t=t_{\max}$ to $t=0$ with $\lambda=\lambda^{\mathrm{c}}=0$ for $t=t_{\max}$ is used. Boundary conditions are:

- for the diffuse adjoint operator λ

$$\lambda\left(\vec{r}_{\mathrm{b}},t,\vec{\Omega}\right)_{\cos(\vec{\Omega},\vec{n})>0}=-\left(F(d^{\mathrm{P}})-F(d^{\mathrm{M}})\right)F'\tau-\int_{\cos(\vec{\Omega}',\vec{n})<0}\mathrm{d}\Omega'\,\lambda\rho\left(\vec{\Omega},\vec{\Omega}'\right)\cos\left(\vec{\Omega}',\vec{n}\right) \tag{16}$$

- for the collimated adjoint operator λ^{c}

$$\lambda^{\mathrm{c}}\left(\vec{r}_{\mathrm{b}}^{\mathrm{c}},t,\vec{\Omega}^{\mathrm{c}}\right)_{\cos\left(\vec{\Omega}^{\mathrm{c}},\vec{n}\right)>0}=-\left(F(d^{\mathrm{P}})-F(d^{\mathrm{M}})\right)F'\tau-\lambda^{\mathrm{c}}\rho\left(\vec{\Omega}^{\mathrm{c}},-\vec{\Omega}^{\mathrm{c}}\right)\cos\left(-\vec{\Omega}^{\mathrm{c}},\vec{n}\right)_{<0}. \tag{17}$$

Once the gradient of the objective function has been determined with the help of an efficient method, a new update of the parameters to be reconstructed is computed following the generic formula:

$$(\kappa,\sigma_{\mathrm{s}})^{k+1}=(\kappa,\sigma_{\mathrm{s}})^{k}+\alpha^{k}\vec{d}^{k} \tag{18}$$

k gives the reconstruction iteration. $\vec{d}^{k}$ is the direction of the line-minimization process on the (κ, σ_{s})-parameter space, provided by the Polack–Ribière method.

In the following, a method for optimizing the descent step size, α^{k}, is proposed, with the help of a Taylor development of the objective function:

$$\begin{aligned}\phi(\kappa+\Delta\kappa,\sigma_{\mathrm{s}}+\Delta\sigma_{\mathrm{s}})=\phi(\kappa,\sigma_{\mathrm{s}})&+\alpha^{k}\int_{T}\mathrm{d}t\int_{\partial D}\mathrm{d}\vec{r}_{\mathrm{b}}\left(F(d^{\mathrm{P}})-F(d^{\mathrm{M}})\right)F'\Delta d^{\mathrm{P}}\\&+\frac{1}{2}\alpha^{k^2}\int_{T}\mathrm{d}t\int_{\partial D}\mathrm{d}\vec{r}_{\mathrm{b}}(F'\Delta d^{\mathrm{P}})^{2}.\end{aligned} \tag{19}$$

The quantities $\Delta\kappa$, $\Delta\sigma_{\mathrm{s}}$ are small variations of the optical parameters, $=\alpha^{k}\vec{d}^{k}$, while Δd is obtained from a perturbation $\vec{d}^{k}$ of those parameters in the sensitivity equations—not shown here—with the same boundary conditions as the tRTE itself.

The descent step size, α^{k}, is sought so that $\varphi(\kappa+\Delta\kappa,\ \sigma_{\mathrm{s}}+\Delta\sigma_{\mathrm{s}})$ is minimized:

$$\frac{\mathrm{d}\phi(\kappa+\Delta\kappa,\sigma_{\mathrm{s}}+\Delta\sigma_{\mathrm{s}})}{\mathrm{d}\alpha}=0\Rightarrow\alpha^{k}=-\frac{\int_{T}\mathrm{d}t\int_{\partial D}\mathrm{d}\vec{r}_{\mathrm{b}}\left(F(d^{\mathrm{P}})-F\left(d^{\mathrm{M}}\right)\right)F'(\partial d^{\mathrm{P}}/\partial(\kappa,\sigma_{\mathrm{s}}))\vec{d}^{k}}{\int_{T}\mathrm{d}t\int_{\partial D}\mathrm{d}\vec{r}_{\mathrm{b}}\left(F'\Delta d^{\mathrm{P}}\right)^{2}} \tag{20}$$

or

$$\alpha^{k}=-\frac{\vec{\nabla}\phi\cdot\vec{d}^{k}}{\int_{T}\mathrm{d}t\int_{\partial D}\mathrm{d}\vec{r}_{\mathrm{b}}(F'\Delta d^{\mathrm{P}})^{2}}. \tag{21}$$

This development has been inherited from inverse design problem methods in thermal transfer and material transformation [24]. The use of the sensitive equation to find an estimate of α^{k} is a good alternative to the Newton–Raphson method where the Hessian matrix is not obtainable, other than through costly finite differences.

3. Results and discussion

In this section, simulations are conducted in order to explore the effect of the boundary conditions on the emerging signal. The level of reflectivity, through the Fresnel laws, varies with the refractive index of the medium (the outside index is unity).

Direct 2-D simulations are first presented on a numerical phantom comparable to the one to be reconstructed, see Fig. 1(a). The blank circles indicate positions where the signal is collected. One is on the path of the collimated beam—position (1). The two others—positions (2) and (3)—are closer to the side of the material and expected to be reached by the light relatively later. Simulations have been conducted on a 25^2 mesh with the S_8 quadrature set of a finite difference discrete ordinate method. A laser pulse of duration $n/(\beta c)$ is injected in the medium whose optical properties are: $\kappa = 50\,\mathrm{m}^{-1}$ and $\sigma_s = 5000\,\mathrm{m}^{-1}$. Two inclusions are embedded, which represent, respectively, an increase and a decrease of 20% in the scattering coefficient with respect to the background value. The overall optical thickness is unity. Figs. 1(b), (c) and (d) show the signal with respect to time for two levels of refractive index $n = 1, 1.33$. The intensity of the laser pulse, I^o, and the mean free path time in the reference medium, $n/(\beta c)$, are used to make the variables dimensionless.

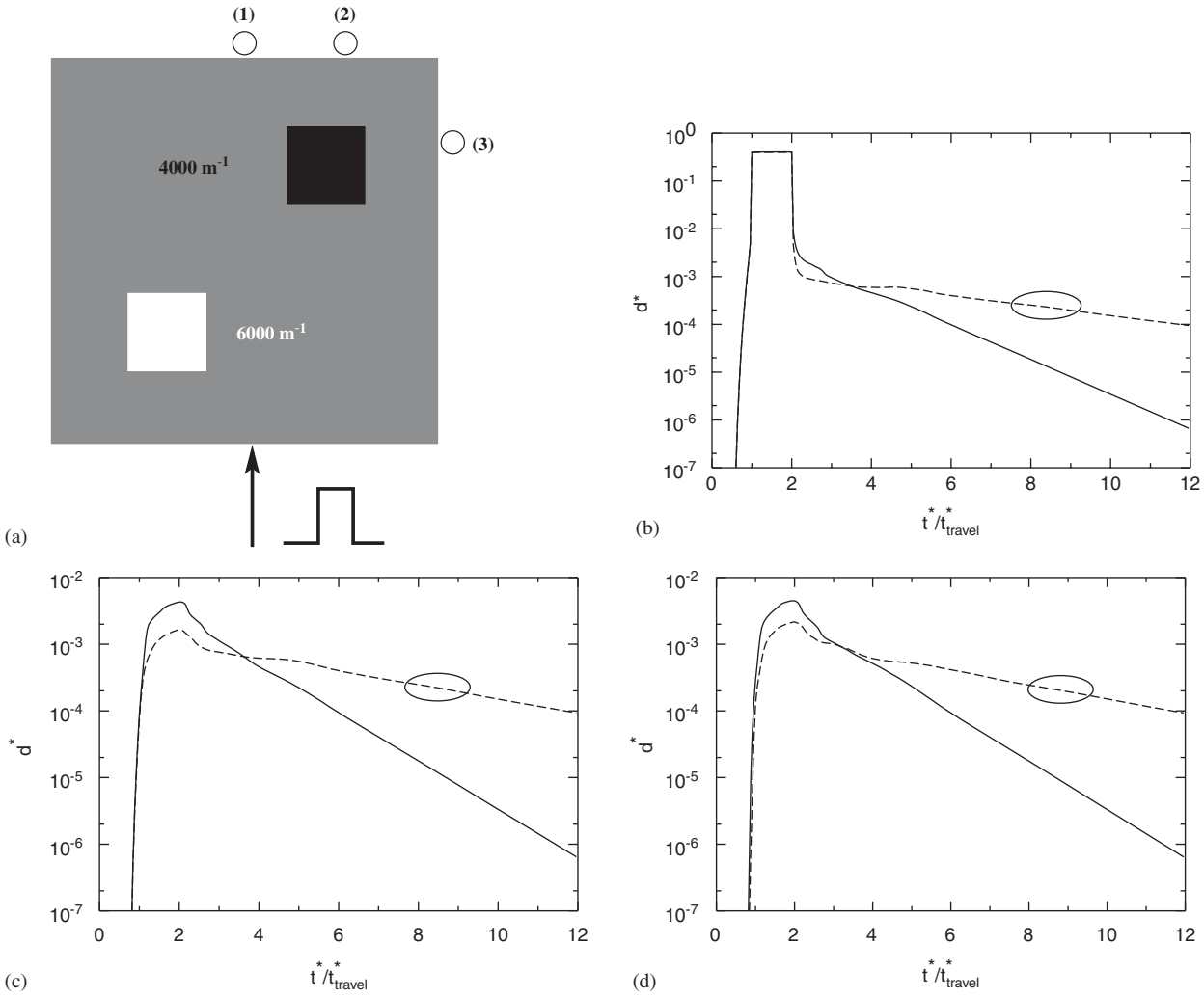

Fig. 1. Temporal signal at detector position: (a) Phantom with location of detectors. (b) Signal from the detector in front of the laser beam (position 1). (c) Signal from the detector on the emergence frontier but not in straight transmission (position 2). (d) Signal from the detector on the side (position 3). Solid line: $n = 1$. Dashed line: $n = 1.33$.

Obviously, more reflection (corresponding to a larger refractive index n) significantly reduces the temporal decay of the signals. It leads to a late establishment of the asymptotic logarithmic regime (ALS), about 10 times the duration for the light to cross the medium (t_{travel}), while only six times for $n = 1$. The ellipses on the figure indicate an area where a subtle change in the slope occurs before reaching the ALS. Although hard to see on the figures, indirect effects have been observed by the authors: simulations with $n = 1.44$ (not presented) have shown that the temporal signature significantly diverges from $n = 1.33$ when entering the ALS in the ellipse area. Reconstructions (see below) have only been consistent when considering that the ALS for $n = 1.33$ and 1.44 (not shown) effectively begins in the ellipse area. This observation provides the estimation of the duration of the simulations to make the reconstruction benefit from all the information present in the detector

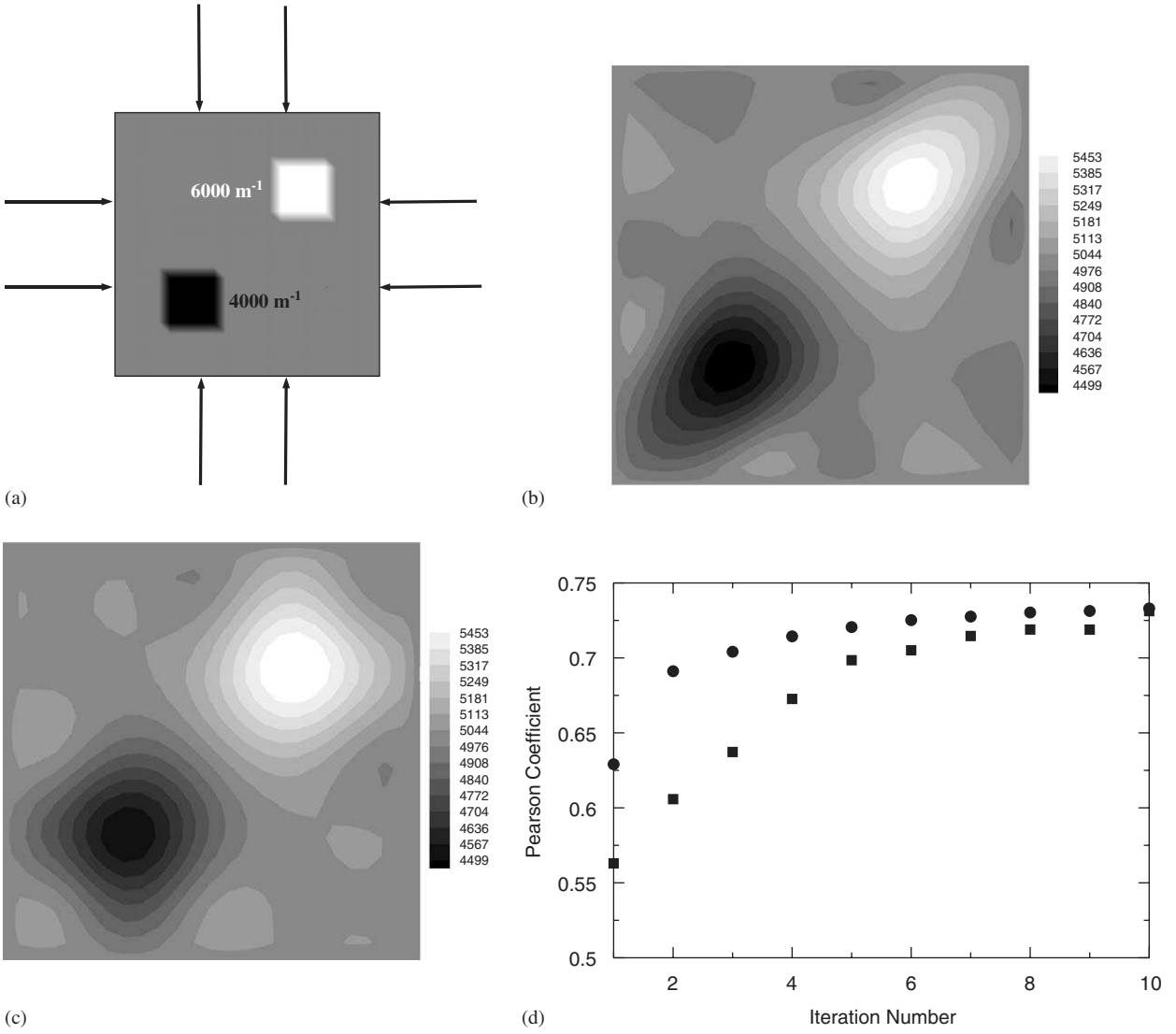

Fig. 2. Inverse imaging: (a) Phantom to be retrieved ($\kappa = 50\,m^{-1}$, background: $\sigma_s = 5000\,m^{-1}$, top inclusion: $\sigma_s = 6000\,m^{-1}$, bottom inclusion: $\sigma_s = 4000\,m^{-1}$). (b) Scattering coefficient distribution reconstruction for $n = 1$ after 10 iterations. (c) Scattering coefficient distribution reconstruction for $n = 1.33$ after 10 iterations. (d) Pearson coefficient for the first 10 reconstruction iterations. Filled squares: $n = 1$. Filled circles: $n = 1.33$.

signatures. Therefore, the time span for the detector readings in the following computations will be 10 times the duration of the light travel across the medium.

For reconstruction attempts, eight laser shots have been sent around the sample whose surfaces are covered by 100 detectors, Fig. 2(a). Reference data are numerically provided. Fig. 2 summarizes the results. Obviously, the reconstruction obtained with reflective boundary conditions ($n = 1.33$) offers a better contrast after 10 iterations, Fig. 2(b) compared to Fig. 2(c), although this performance is somewhat damaged by regularization. The trends given by the Pearson coefficient $(\sum_i(\sigma_{s_i}^o - \bar{\sigma}_s^o)(\sigma_{s_i} - \bar{\sigma}_s)) \Big/ \sqrt{\sum_i(\sigma_{s_i}^o - \bar{\sigma}_s^o)^2} \Big/ \sqrt{\sum_i(\sigma_{s_i} - \bar{\sigma}_s)^2}$, where superscripts 'o' and '-' denote the known distribution and the mean value, respectively, and i counts the scattering coefficients discretized on the uniform mesh), Fig. 2(d), are very interesting as they suggest that reflective boundary conditions not only improve the final image but also allow to reconstruct it in fewer iterations. Boundary reflection improves the chances of carrying more information for photons arriving at the detectors. These results indicate that reflecting boundary can be a good candidate to speed up the reconstruction.

Long-time photons filtering is not available in case of steady-state and frequency-domain optical tomography, two techniques expected to be cheaper and easier than time-domain optical tomography. Increasing the reflectivity at the boundary of the sample to be probed would be thus an interesting avenue to prolong the duration of the photons in the sample, bringing a lot of information. Developments are currently undertaken to explore these possibilities.

References

[1] Louis A. Medical imaging: state of the art and future development. Inverse Probl 1992;8:709–38.
[2] Hebden J, Wong K. Time resolved optical tomography. Appl Opt 1993;32:372–80.
[3] Wang L, Ho P, Alfano R. Time-resolved Fourier spectrum and imaging in highly scattering media. Appl Opt 1993;32:5043–8.
[4] Delpy D, Cope M, Van Der Zee P, Arridge S, Wray S, Wyatt J. Estimation of optical pathlength through tissue from direct time of flight measurement. Phys Med Biol 1988;33:1433–42.
[5] Jiang H, Paulsen K, Osterberg U. Optical image reconstruction using DC data: simulations and experiments. Phys Med Biol 1996;41:1483–98.
[6] Klose A, Hielscher A. Fluorescence tomography with simulated data based on the equation of radiative transfer. Opt Lett 2003;28:1019–21.
[7] Klose A, Ntziachristos V, Hielscher A. The inverse source problem based on the radiative transfer equation in optical molecular imaging. J Comput Phys 2005;202:323–45.
[8] Arridge S, Schweiger M. A gradient-based optimisation scheme for optical tomography. Opt Express 1998;2:213–26.
[9] Klose A, Netz U, Beuthan J, Hielscher A. Optical tomography using the time-independent equation of radiative transfer—Part 1: forward model. JQSRT 2002;2:691–713.
[10] Klose A, Hielscher A. Optical tomography using the time-independent equation of radiative transfer—Part 2: inverse model. JQSRT 2002;72:715–32.
[11] Schweiger M, Arridge S. Application of temporal filters to time resolved data in optical tomography. Phys Med Biol 1999;44:1699–717.
[12] Arridge S. Optical tomography in medical imaging. Inverse Probl 1999;15:41–93.
[13] Klose A, Hielscher A. Iterative reconstruction scheme for optical tomography based on the equation of radiative transfer. Med Phys 1999;26:1698–707.
[14] Dorn O. A transport-backtransport method for optical tomography. Inverse Probl 1998;14:1107–30.
[15] Haskell R, Svaasand L, Tsay T, Feng T, McAdams M, Tromberg B. Boundary conditions for the diffusion equation in radiative transfer. J Opt Soc Am A 1994;11:2727–41.
[16] Hielscher A, Klose A, Scheel A, Moa-Anderson B, Backhaus M, Netz U, et al. Sagittal laser optical tomography for imaging of rheumatoid finger joints. Phys Med Biol 2004;49:1147–63.
[17] Ren K, Abdoulaev G, Bal G, Hielscher A. Algorithm for solving the equation of radiative transfer in the frequency domain. Opt Lett 2004;29:578–80.
[18] Boulanger J, Charette A. Numerical developments for short-pulsed near infra-red laser spectroscopy. Part I: direct treatment. JQSRT 2005;91:189–209.
[19] Boulanger J, Charette A. Numerical developments for short-pulsed near infra-red laser spectroscopy. Part II: inverse treatment. JQSRT 2005;91:297–318.
[20] Arridge S, Hebden J. Optical imaging in medicine: II. Modelling and reconstruction. Phys Med Biol 1997;42:841–53.
[21] Ramankutty M, Crosbie A. Modified discrete ordinates method of radiative transfer in two-dimensional rectangular enclosures. JQSRT 1997;57:107–40.

[22] Sakami M, Charette A. Application of a modified discrete ordinates method to two-dimensional enclosures of irregular geometry. JQSRT 2000;64:275–98.
[23] Sakami M, El Kasmi A, Charette A. Analysis of radiative heat transfer in complex two-dimensional enclosures with obstacles using the modified discrete ordinates method. ASME J Heat Transfer 2001;123:892–900.
[24] Zabaras N, Kang S. On the solution of an ill-posed design solidification problem using minimization techniques in finite- and infinite-dimensional function spaces. Int J Numer Meth Eng 1993;36:3973–90.